SCIENTIFIC REPORTS

OPEN

SUBJECT AREAS:
PHOTONIC DEVICES
ELECTRONIC MATERIALS
ELECTRONIC DEVICES
SENSORS

Received
19 February 2014

Accepted
28 April 2014

Published
9 June 2014

Correspondence and requests for materials should be addressed to J.L. (jbli@semi.ac.cn)

Photoresponsive and Gas Sensing Field-Effect Transistors based on Multilayer WS_2 Nanoflakes

Nengjie Huo[1], Shengxue Yang[1], Zhongming Wei[2], Shu-Shen Li[1], Jian-Bai Xia[1] & Jingbo Li[1]

[1]State Key Laboratory for Superlattices and Microstructures, Institute of Semiconductors, Chinese Academy of Sciences, P.O. Box 912, Beijing 100083, China, [2]Nano-Science Center & Department of Chemistry, University of Copenhagen, Universitetsparken 5, DK-2100 Copenhagen Ø, Denmark.

The photoelectrical properties of multilayer WS_2 nanoflakes including field-effect, photosensitive and gas sensing are comprehensively and systematically studied. The transistors perform an n-type behavior with electron mobility of 12 cm^2/Vs and exhibit high photosensitive characteristics with response time (τ) of $<$20 ms, photo-responsivity (R_λ) of 5.7 A/W and external quantum efficiency (EQE) of 1118%. In addition, charge transfer can appear between the multilayer WS_2 nanoflakes and the physical-adsorbed gas molecules, greatly influencing the photoelectrical properties of our devices. The ethanol and NH_3 molecules can serve as electron donors to enhance the R_λ and EQE significantly. Under the NH_3 atmosphere, the maximum R_λ and EQE can even reach 884 A/W and 1.7 $\times$ 10^5%, respectively. This work demonstrates that multilayer WS_2 nanoflakes possess important potential for applications in field-effect transistors, highly sensitive photodetectors, and gas sensors, and it will open new way to develop two-dimensional (2D) WS_2-based optoelectronics.

Graphene, the monolayer counterpart of graphite, has attracted extensive attention in recent years because of its unusual electrical, optical, magnetic and mechanical properties[1–4]. It displays an exceptionally high carrier mobility exceeding 10^6 $cm^2\,V^{-1}\,s^{-1}$ at 2 K and 15000 $cm^2\,V^{-1}\,s^{-1}$ at room temperature[5,6], and the linear dispersion of the Dirac electrons near the K point makes graphene be used as photodetector with high operation frequencies[7] and ultrawide band operation[8]. However, the zero bandgap of graphene limits its applications in optoelectronics, for example, field-effect transistors (FETs) based on graphene cannot be effectively switched off due to the high OFF-currents. In contrast, 2D transition metal dichalcogenides (TMDCs) with chemical formula MX_2 (M = Mo, W, Ga, *etc.* and X = S, Se or Te) possess sizable bandgaps[9,10] around 1–2 eV, which attracted widely interest due to their interesting physical properties and applications in nanoelectronics, sensing and photonics[11–16]. Particularly, the 2D TMDCs based FETs, photodetectors and gas sensors have been extensively studied. As one earliest TMDCs used in FETs, WSe_2 crystal[17] shows high mobility ($>$500 $cm^2\,V^{-1}\,s^{-1}$), ambipolar behavior and 10^4 on/off ratio at 60 K. Afterwards, mono or few-layer MoS_2 FETs with a back-gated[18] and top-gated configuration[19] are reported to exhibit an excellent on/off ratio ($\sim10^8$) and room-temperature mobility of $>$ 200 $cm^2\,V^{-1}\,s^{-1}$. Although the high photodetection performance, several problems such as very low responsivity ($\sim10^{-2}$ A/W) and external quantum efficiency (0.1–0.2%) still remain with graphene photodetectors[20,21]. Compared to graphene-based devices, photodetectors made from TMDCs thin layers can exhibit enhanced responsivity and selectivity. For example, a few-layer MoS_2 photodetector is demonstrated with improved responsivity (0.57 A/W) and fast photoresponse[11] ($\sim$70–110 μs), and the monolayer MoS_2-based devices[22] show a maximum photoresponsivity of 880 A/W. Recently, 2D GaS and GaSe thin nanosheets are also reported as high performance photodetectors[13,14,23,24]. Moreover, TMDCs suggest opportunities in molecular sensing applications due to the high surface-to-volume ratio. For instance, single and few-layer MoS_2 sheets have been demonstrated to be sensitive detectors for NO, NO_2, NH_3 and triethylamine gas[25–28]. The detection mechanism is probably due to the n-doping or p-doping induced by the adsorbed gas molecular, changing the resistivity of the intrinsically n-doped MoS_2. However, as a typical member of 2D TMDCs materials, WS_2 thin layers are less studied on their photoelectrical properties. Particularly, no research has been reported for the potential application of WS_2 in photodetector and gas sensors. Actually, WS_2 possesses some advantages compared to MoS_2. For example, MoS_2 is usually procured from natural sources with no control over contaminations. WS_2 exhibits higher thermal stability[29] and wider operation temperature range as lubricants[30]. A

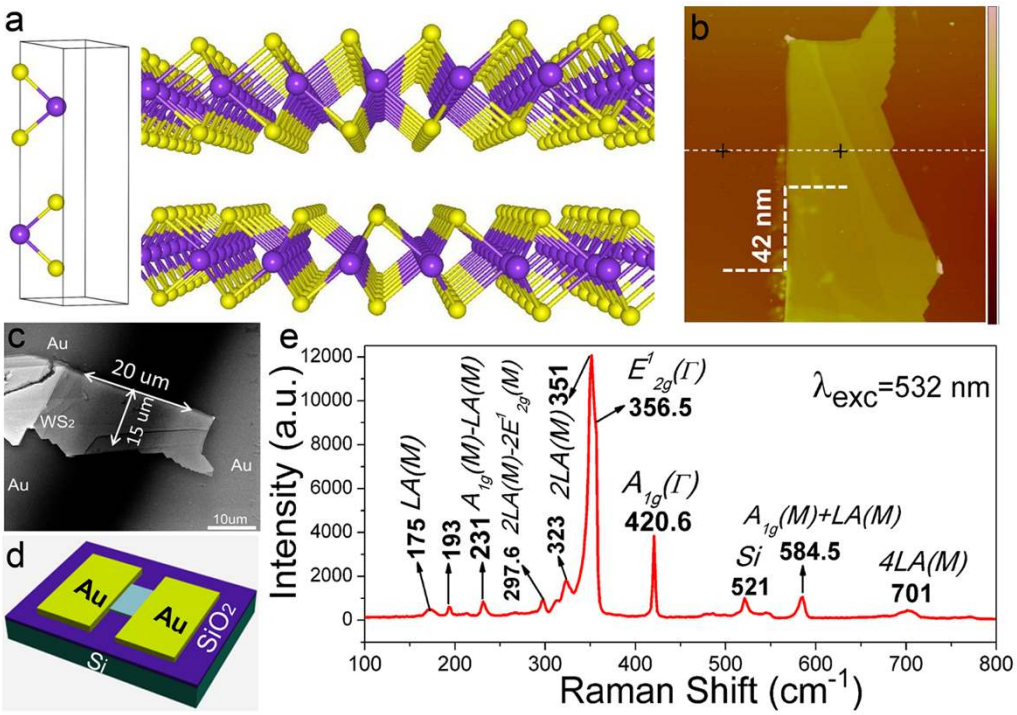

Figure 1 | Characterization of the multilayer WS_2 nanoflakes. (a) Primitive cell and three-dimensional schematic representation of a typical WS_2 structure with the sulfur atoms in yellow and the tungsten atoms in purple. Atomic force microscopy (AFM) image (b) and scanning electron microscopy (SEM) image (c) of the actual transistor based on multilayer WS_2 nanoflakes. (d) Schematic diagram of the device. The thickness of WS_2 nanoflakes is 42 nm. The width (W) and length (L) of the channel in the device is 15 μm and 20 μm, respectively. (e) Room-temperature Raman spectrum from the multilayer WS_2 nanoflakes, using the 532 nm laser.

recent calculation also shows that single layer WS_2 has the potential to outperform other 2D crystals in FETs applications due to its favorable bandstructure[31], and the transistors based on chemically synthesized layered WS_2 is also reported to exhibit 10^5 room temperature modulation and ambipolar behavior[32].

In this paper, multilayer WS_2 nanoflakes are exfoliated from the commercially available WS_2 crystals (Lamellae Co.) onto 300 nm SiO_2/Si substrates using conventional mechanical exfoliation technique. The multilayer WS_2 nanoflakes transistors show excellent field-effect properties with a high electron mobility of 12 cm^2/Vs and high sensitive to red light (633 nm) with R_λ (defined as the photocurrent generated per unit power of the incident light on the effective area) of 5.7 A/W and high EQE (defined as the number of photo-induced carriers detected per incident photons) of 1118%, indicating the 2D WS_2 will be a new promising material for high performance photodetectors. Moreover, the sensing of various gas molecules on this transistor is preliminary investigated for the first time. We find strong response upon exposure to reducing gas of ethanol and NH_3, which can serve as electron donors, enhancing n-type and conductivity of WS_2 nanoflakes. On the contrary, the oxidizing gas of oxygen can act as electron acceptors to withdraw substantial electrons from the WS_2 nanoflakes, depleting its n-type and reducing the conductivity. We also observe the enhanced R_λ and prolonged response to the reducing gas, caused by temporary charge perturbation in the WS_2 nanoflakes from the adsorbed electron donors. Remarkably, the maximum R_λ of the device can reach 884 A/W under light illumination of 50 μW/cm^2 at the NH_3 atmosphere, which is 10^6 times higher than the first graphene-based photodetectors[7] and 10^5 times higher than previous reports for monolayer MoS_2 phototransistors[33]. Here, the excellent electrical, photosensitive and gas sensing properties of the multilayer WS_2 nanoflakes transistors are studied systematically, suggesting great potential practical applications in FETs, photodetectors and gas sensors.

Results

Characterization of multilayer WS_2 nanoflakes. Bulk WS_2 is an indirect-bandgap (1.4 eV) semiconductor, but can turn into a direct-bandgap (2.1 eV) material when exfoliated into the monolayer state[34]. Each single plane of WS_2 comprises a trilayer composed of a tungsten layer sandwiched between two sulfur layers in a trigonal prismatic coordination as shown in Figure 1a. The multilayer WS_2 nanoflakes based transistors were fabricated with a coplanar electrode geometry by "gold-wire mask moving" technique[35,36]. Through the AFM (Figure 1b and Figure S1) and SEM (Figure 1c) images of actual devices with SiO_2 as bottom gating, the thickness of the WS_2 nanoflakes is about 42 nm, and the width and length of the channel are 20 μm and 15 μm, respectively. Figure 1d shows the schematic diagram of the device. EDX (Figure S2) results indicate the existence of S and W elements with an atom ratio of 2 in the WS_2 nanoflakes.

The first-order Raman spectra of the WS_2 nanoflakes showed two optical phonon modes at the Brillouin zone center ($E^1_{2g}(\Gamma)$ and $A_{1g}(\Gamma)$) and one longitudinal acoustic mode at the M point (LA(M)). $E^1_{2g}(\Gamma)$ was an in-plane optical mode, $A_{1g}(\Gamma)$ corresponded to out-of-plane vibrations of the sulfur atoms, and the longitudinal acoustic phonons LA(M) were in-plane collective movements of the atoms (Figure S3). Raman spectra of the WS_2 nanoflakes were performed with the 532 nm laser excitations (Figure 1e). The first-order Raman peaks are identified at 175, 356.5 and 420.6 cm^{-1}, which are attributed to the LA(M), $E^1_{2g}(\Gamma)$ and $A_{1g}(\Gamma)$ modes, respectively. Additional peaks correspond to the second-order Raman modes which are multiphonon combinations of these first-order modes. Our Raman results for the multilayer WS_2 nanoflakes agree well with the previous reports[37–39].

Electrical properties under dark and light illumination. Owing to the lack of dangling bonds, structural stability and high mobility[40], 2D TMDCs were promising materials for FETs. To evaluate the

electrical performance of the multilayer WS_2 nanoflakes, the bottom-gated transistors on SiO_2/Si were fabricated. Figure 2a and 2b show the typical output and transfer characteristics respectively, performing an n-type behavior. According to the previous reports[41,42], in the case of $V_G > V_T$ and $|V_{DS}| \ll |V_G - V_T|$, the FETs are turned on. The positive gate voltage (V_G) can induce large amounts of electrons in the interfaces between the WS_2 nanoflakes and SiO_2 substrate, and a conducting channel is created which allows the current to flow between the source and drain. The FETs operate like a resistor and work at linear region, thus the source-drain current (I_{DS}) can linearly depend of source-drain voltage (V_{DS}) as shown in the inset of Figure 2a. In this case, the I_{DS} and V_{DS} can satisfy the formula $I_{DS} = \frac{W}{L}\mu C_i(V_G - V_T)V_{DS}$, where L is channel length (20 μm), W is channel width (15 μm), and C_i is the gate capacitance which can be given by equation $C_i = \varepsilon_o\varepsilon_r/d$, ε_o (8.85×10^{-12} F/m) is vacuum dielectric constant, and ε_r (3.9) and d (300 nm) are dielectric constant and thickness of SiO_2, respectively. The field-effect carrier mobility (μ) and threshold voltage (V_T) of WS_2 nanoflakes based FETs can be calculated from the linear region of the output properties by supplying the values of I_{DS} and V_{DS} at different V_G into the above equation. We get that $V_T = -3.5$ V, and the electrons mobility is up to 12 cm^2/Vs. To estimate the intrinsic doping level of the prepared WS_2 nanoflakes, I_{DS} at zero V_G was modeled as $I_{DS} = qn_{2D}W\mu(\frac{V_{DS}}{L})$, where n_{2D} is the 2D carrier concentration, q is the electron charge. From the output characteristics of WS_2 nanoflakes (Figure 2a), n_{2D} is extracted to be $\sim 1.4 \times 10^{11}$ cm^{-2}. We have also performed Hall-effect measurements with four-probes on the WS_2 nanoflakes to accurately determine μ and n_{2D}, and the results are very similar with the field-effect μ and n_{2D} (Figure S4).

The multilayer WS_2 nanoflakes FETs were also illuminated with white light from LED and red light from red laser, and the output characteristics of the devices are shown in Figure 2c and 2d, respectively. The transfer characteristic curves under dark and light are shown in Figure 2e. The curves are obviously improved under both white and red light illumination, indicating the photosensitive property to the visible light. As discussed above, our prepared WS_2 nanoflakes perform n-type behavior with an intrinsic density of electrons of about 1.4×10^{11} cm^{-2}. The carriers density can be modulated by supplying the electrical gating, which can be explained simply using the parallel-plate capacitor model. When positive V_G is added on the bottom of dielectric (SiO_2), much electrons will be induced in the interface between WS_2 nanoflakes and SiO_2, serving as conductive channel and increasing the drain current. In contrast, negative V_G will deplete the electrons in the interface and reduce the drain current. In addition, the increased V_{DS} can increase the carrier drift velocity and reduce the carrier transit time T_t (defined as $T_t = L^2/\mu V_{DS}$), thus contributing to the increased drain current (Figure 2e and 2f). Table 1 show the V_T, μ and n_{2D} under dark and light illumination for the multilayer WS_2 nanoflakes, which are extracted from the linear region of output characteristics. We found that the absolute values of V_T, μ and n_{2D} are all increased under light illumination. The photo-generated carriers contribute to the increased electrons density resulting in that larger negative voltage is needed to deplete them. The electron mobility (μ) can be obtained from the equation $\mu = \frac{\partial I_{DS}}{\partial V_G}(\frac{L}{WC_iV_{DS}})$, the source drain current I_{DS} and current change between ON and OFF states are increased under light illumination, leading to the increased slope of $\partial I_{DS}/\partial V_G$, and hence enhancing the calculated mobility.

Photodetector based on WS_2 nanoflakes. Few- or monolayer MoS_2 was demonstrated as ultrasensitive photodetectors based on the previous reports[11,22,43]. In contrast to the widely studied MoS_2 used for photodetectors, little attention has been paid to the 2D WS_2. According to the above analysis, the multilayer WS_2 nanoflakes can response to the visible light especially the red light with

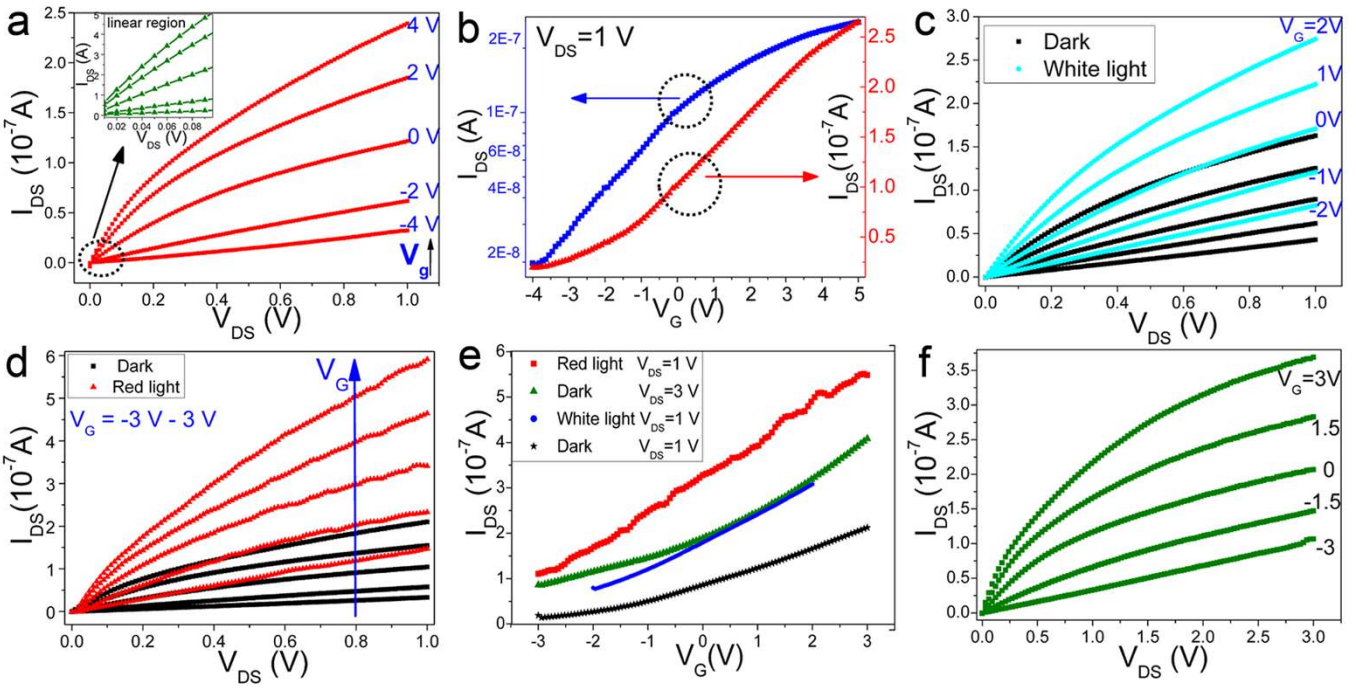

Figure 2 | Field effect of the multilayer WS_2 nanoflakes. (a) Output characteristics of the transistor based on multilayer WS_2 nanoflakes using Au/Au as the drain/source electrodes. The inset is linear region at low source drain voltage. (b) Transfer characteristics of the device at a fixed V_{DS} of 1 V on a log scale (left y axis) and on a linear scale (right y axis). All measurements were performed in air at room temperature with the absence of light. Output characteristics of the device with (c) white light (15 mW/cm^2) from LEDs and (d) red light (633 nm, 15 mW/cm^2) from red lasers. (e) Transfer characteristics of the devices in dark and under light illumination. (f) Output characteristics of the devices in dark with V_{DS} ranging from 0 to 3 V.

Table 1 | Threshold voltage (V_T), electron mobility (μ), and density of electrons (n_{2D}) of a typical transistor under dark and light illumination

Parameters	V_T (V)	μ (cm^2/Vs)	n_{2D} (10^{10} cm^{-2})
Dark	−3.5	12	9.4
White light	−3.6	19.7	11
Red light	−4	25	17

633 nm since the energy of the red light approximates the band gap of WS_2. Therefore, the photosensitive properties of the WS_2 nanoflakes based photodetctors for the red light was measured systematically. Figure 3a shows the output characteristics under chopped red light irradiation with zero V_G. The drain current can be modulated rapidly by the chopped light, and the current is significantly increased under the light irradiation compared to that in dark, implying a quick response to red light. As shown in Figure 3b, with light irradiation on/off, the device can work between low and high impedance states fast and reversibly with an on/off ratio (defined as I_{photo}/I_{dark}) of 25, allowing the device to act as a high quality photosensitive switch. The device also exhibits very fast dynamic response for both rise and decay process (Figure 3c), the response and recovery time is shorter than the detection limit of our measurement setup (20 ms), which is shorter than values for phototransistors based on monolayer MoS_2 and hybrid graphene quantum dot[22,44], and it is also orders of magnitude shorter than the amorphous oxide semiconductors phototransistors[45]. Stability test of photo-switching behavior of the WS_2 nanoflakes is also performed by switching the light on/off quickly and repetitively, accordingly the photocurrent of the device can change instantly between "ON" state and "OFF" state (Figure 3d). After hundreds of cycles, the photocurrent can still change with light switching on/off, displaying a high reversibility and stability of the device. Figure 3e shows the output characteristics under different light illumination densities. When the WS_2 nanoflakes absorb the incident photons, large amounts of electron-pairs generate, forming like a conductive channel, and then being extracted by V_{DS} to form the photocurrent. With increasing light density, the photocurrent is increased significantly. From the "output" characteristics shown in Figure 3f, our phototransistor can be open by the incident light of about 10 mW/cm^2. So, like the electrical field effect, the incident light field can also act as a "gating" to modulate the density of carries in the source drain channel and make important effect on the electrical properties of the device.

Gas sensing and its effect on photoresponse. Previous reports showed that the photoelectrical response properties were strongly affected by gas environment for the MoS_2 monolayer-based phototransistors[43]. We also performed the photosensitive measurements of our devices in ambient air and under vacuum. The drain current under vacuum is higher than that in ambient air under both dark and light (Figure 4a), and the increment of current is more obvious under light illumination shown in the inset. Moreover, the photosensitivity is also enhanced under vacuum (Figure 4b). Density functional theory (DFT) calculations[12] discover that the O_2 and H_2O molecules can interact weakly to the TMDCs monolayer with binding energies ranging from 70 to 140 meV and substantial electrons can transfer into the physical-adsorbed gas molecules from the semiconductors. Large amounts of O_2 and H_2O molecules exist in air and the WS_2 nanoflakes display n-type behavior from the above Hall and field-effect results. In our case, O_2 and H_2O molecules in ambient air can be physically adsorbed on the surface of the WS_2 nanoflakes and withdraw numerous electrons from WS_2, depleting the n-type of WS_2 nanoflakes. Thus the resistance becomes larger due to the reduction of major conduction electrons,

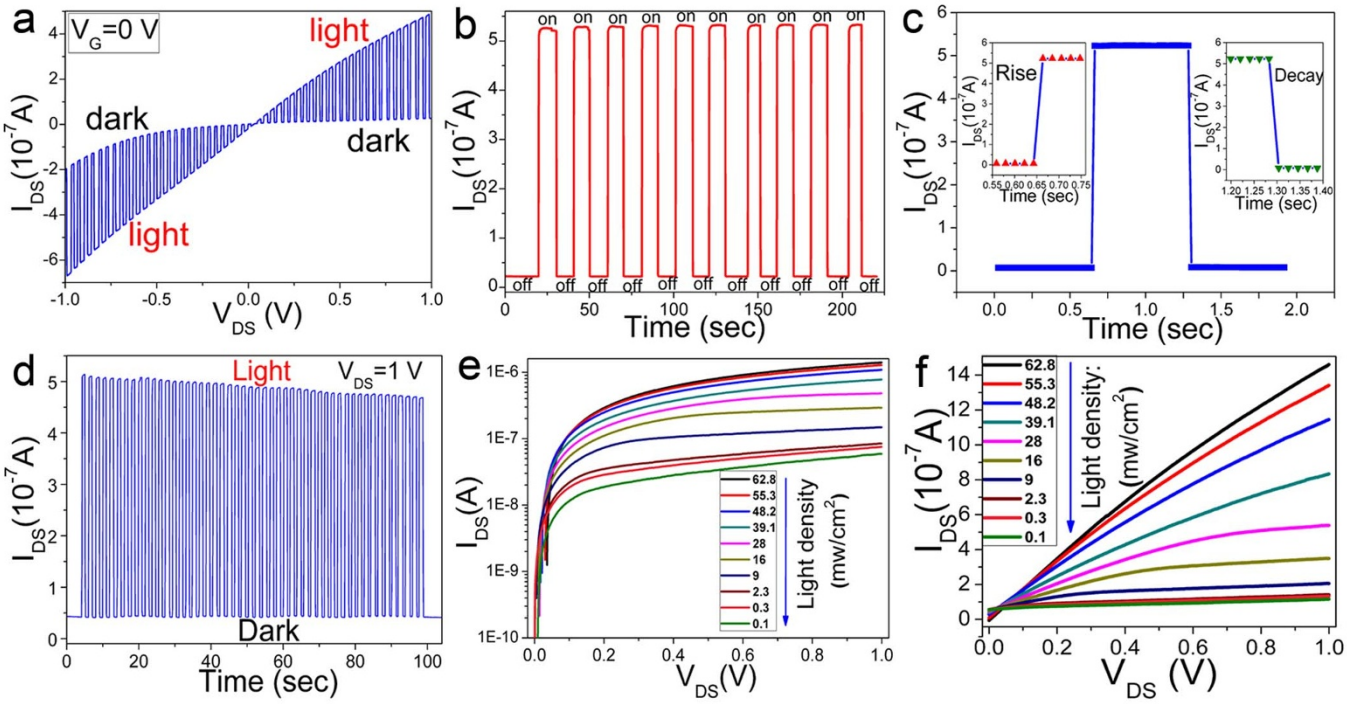

Figure 3 | The performance of the multilayer WS_2 nanoflakes as photodetector. (a) Drain-source (I_{DS}-V_{DS}) characteristic of the device based on the WS_2 nanoflakes under the chopped red light illumination (633 nm, 30 mW/cm^2). (b) Time-dependent photocurrent response during the light switching on/off at source drain voltage of 1.0 V. (c) Dynamic response characteristic of the device. The inset is corresponding to the rise (left) and decay (right) process. (d) Stability test of photo-switching behavior of the device with light switching on/off quickly and repetitively. (e) Source-drain (I_{DS}-V_{DS}) characteristics of the device under different incident optical power density from 0.1 to 62.8 mW/cm^2 on a log scale. (f) "Output" characteristics of the device with light as "gating".

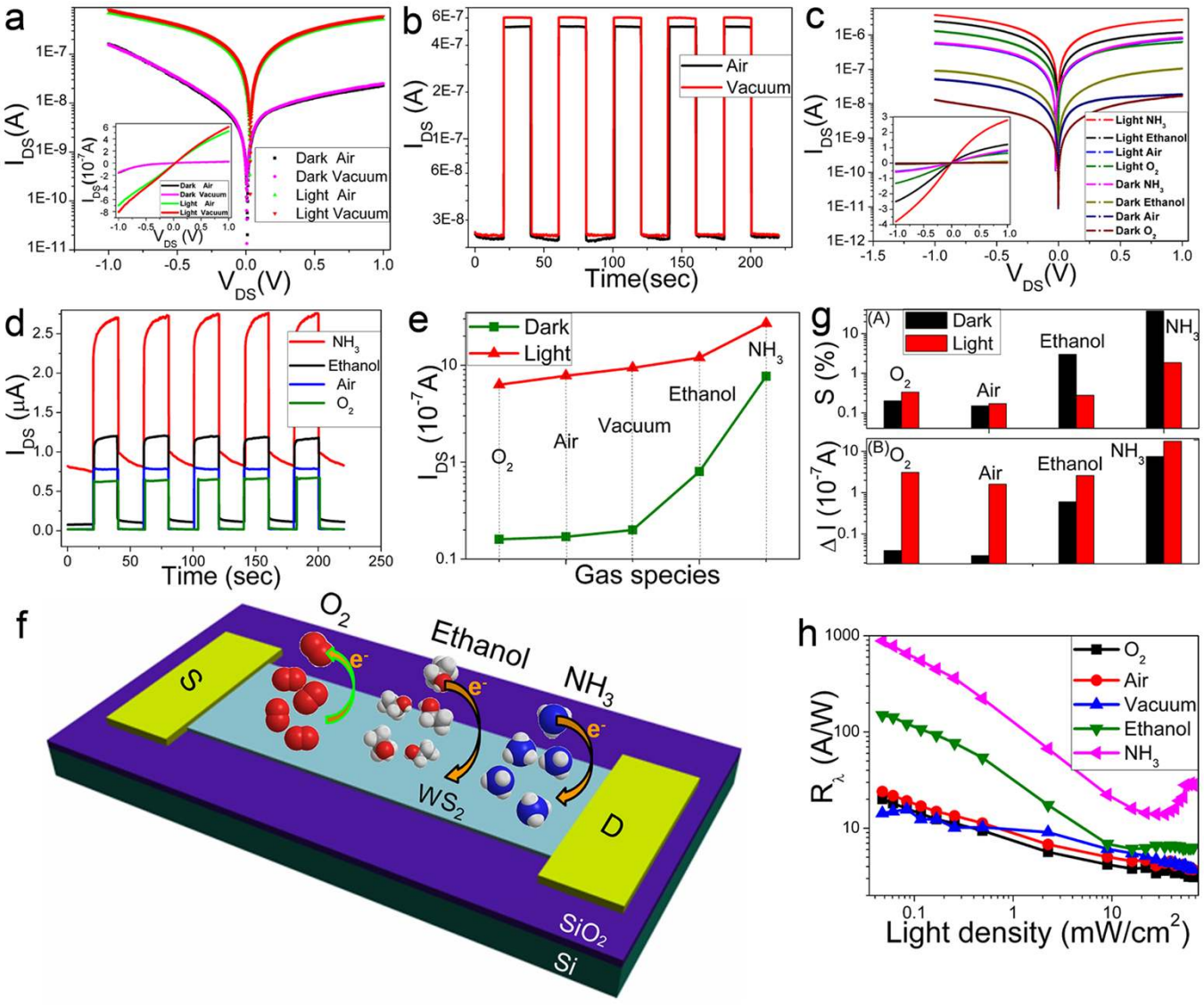

Figure 4 | Gas sensing and its effect on photoresponse. (a) I_{DS}-V_{DS} characteristics (on a log scale of y-axis) of the WS_2 nanoflakes photodetectors under dark or in the presence of light (633 nm, 30 mW/cm^2) measured in air and in vacuum. The insert is corresponding curve on a linear scale of y axis. (b) Time-dependent photocurrent response under air and vacuum during the light switching on/off. (c) I_{DS}-V_{DS} characteristics (on a log scale of y-axis) of the device under dark or in the presence of light (633 nm, 40 mW/cm^2) measured in various gas atmospheres. The inset is corresponding curves on a linear scale of y axis. (d) Time-dependent photocurrent response under various gas atmospheres. (e) The extracted dark current and photocurrent under different gas atmospheres. (f) Schematic diagram of charge transfer process between adsorbed gas molecules and the multilayer WS_2 nanoflakes transistor. (g) The gas sensitivity (A) (defined as $S = |(I_{gas} - I_{vacuum})/I_{vacuum}|$) and current change (B) (defined as $\Delta I = |I_{gas} - I_{vacuum}|$) under different conditions. (h) The photo-responsivity R_λ under various gas atmospheres, showing high sensitivity. The device exhibits a maximum R_λ of 884 A/W with low light density of 50 μW/cm^2.

corresponding to the reduced I_{DS}. Upon light illumination in air, much electron-hole pairs generate and the density of electrons in the WS_2 nanoflakes is improved as discussed above. O_2 and H_2O molecules as electron acceptors will have more electrons to accept, corresponding to more gas molecules in ambient can be adsorbed and deplete more electrons, leading to the decreased photosensitivity. Moreover, the photocurrent shows a strong dependence on light intensity and the experimental data are fitted by a power equation $I_{ph} = aP^{\alpha}$, where a is scaling constant, and α is exponent. Under vacuum, the photocurrent displays a power dependence of ~0.91 (function: $I_{ph} = 0.26P^{0.91}$) as shown in Figure S5a, indicating a superior photocurrent capability and a high efficiency of photo-generated charge carriers from the absorbed photons. However, the exponent α in air (function: $I_{ph} = 0.52P^{0.73}$) shown in Figure S5b is smaller than that under vacuum, indicating the route of the loss of the photo-exited carrier by the adsorbed O_2 or H_2O molecules in air. Similar phenomenon is also observed in MoS_2-based phototransistor[43].

To further investigate the gas effect on the electrical and photosensitive properties of the multilayer WS_2 nanoflakes, the devices were placed in various gas environments during photoelectrical measurements. From the $I_{DS} - V_{DS}$ characteristics (Figure 4c) and time-dependent photocurrent response at various gas atmospheres during the light switching on/off (Figure 4d), the WS_2 nanoflakes can obviously response to the given gas molecules which play an important and different roles in the conductivity and photosensitive properties of the devices. Figure 4e summarizes the drain current under these gas molecules both in dark and under light illumination, the drain current of the device is decreased in O_2 and air, but increased in ethanol and NH_3, compared to that under vacuum. The current

change is considered to result from the charge transfer between the WS_2 nanoflakes and the adsorbed gas molecules as shown in Figure 4f. Once the vapor molecules come into contact with the surface of WS_2, the gas molecule is expected to be adsorbed and subsequently change the charge carrier distribution in WS_2 nanoflakes. O_2 molecules can act as electron acceptors to accept electrons from WS_2, leading to a reduction in overall conductivity. In contrast, ethanol and NH_3 molecules, serving as electron donors, can donate electrons to the WS_2 nanoflakes, which enhance the total conducting electrons density, resulting in the increased current. The gas sensitivity is defined as $S = |(I_{gas} - I_{vacuum})/I_{vacuum}|$, where I_{gas} is current of the device in target gas, and I_{vacuum} is current under vacuum, V_{DS} are 1 V. Figure 4g (A) shows the gas sensitivity of the device under different gas molecules. S is negative higher in O_2 than that in air, because of the higher concentration of O_2 acting as electron acceptor to deplete electrons. On the contrary, the ethanol and NH_3 molecules can act as electron donors to increase electrons in WS_2, displaying a positive S. Particularly, the sensitivity of NH_3 is much higher than that of other gas molecules, indicating the WS_2 nanoflakes are more sensitive to NH_3. Interestingly, we notice that the gas sensitivity of ethanol and NH_3 measured in dark is higher than that under light, but lower for O_2 and ambient air, the possible reason has been described in Supporting Information. In addition, the current change ΔI caused by gas adsorption represents the amounts of adsorbed gas molecules to some extent shown in Figure 4g (B). Obviously, both oxidizing (O_2) and reducing (NH_3, ethanol) gas molecules are easier to be adsorbed in the WS_2 nanoflakes under light illumination compared to under dark, ascribed to the redundant photo-excited electrons or holes.

Furthermore, the exponent α in O_2 ($I \sim P^{0.62}$, Figure S6a) becomes very small, indicating the photo-excited carriers are continuously consumed by the adsorbed O_2 molecules with increasing light density. However, in ethanol ($I \sim P^{1.02}$, Figure S6b) and NH_3 ($I \sim P^{2.5}$, Figure S6c), the α is significantly enhanced, implying a high efficiency of photo-generated charge carriers, attributed to that more reducing gas (ethanol or NH_3) molecules can be adsorbed with increasing incident light density and more electrons can transfer from these adsorbates into the device. Thus, two physical processes upon light illumination including generation of photo-excited electrons and charge transfer from the adsorbed gas molecules can lead to the enhanced charge carrier density, demonstrating a high efficiency of photo-generated carriers. Figure 4h shows the R_λ acquired at different light power densities. At low illumination power density (50 $\mu W/cm^2$) under NH_3 atmosphere, the device reaches a high R_λ of 884 A/W and EQE of 1.7×10^5 %. The R_λ shows a monotonous decrease with increasing illumination intensity due to the saturation of trap states in the WS_2 nanoflakes, which is similar with the MoS_2-based photodetectors[22]. While, at high light powers under the ethanol and NH_3 atmosphere, the R_λ presents a slight increase trend with increasing illumination intensity, further confirming that more reducing gas molecules can be adsorbed and transfer more electrons into the device under high illumination power. Moreover, the presence of gas molecules can also affect the dynamic response of the device, which is discussed in detail in Supporting Information (Figure S7). Briefly, unlike the single exponential formula for fitting the rise and fall photocurrent in other reports[14,46], the dynamic response for rise and fall in our device under the reducing atmosphere (ethanol and NH_3) can be perfectly fitted by double exponential formula, further indicating the existence of two physical mechanisms including rapid generation or recombination of photo-excited electron-hole pairs and gas adsorption or charge transfer process in the dynamic response to the light switching on/off.

Discussion

Based on the above experimental results, the multilayer WS_2 nanoflakes exhibit n-type behavior with relatively large electron mobility of 12 cm^2/Vs, which is much higher than the CVD-grown monolayer WS_2 ($\mu = 0.01$ cm^2/Vs) by three orders of magnitude[47] and comparable to the widely studied few- or monolayer MoS_2 ($\mu = 0.1$–10 cm^2/Vs) fabricated without high-κ dielectrics[19,47,48], but smaller than the top-gated transistors based on the monolayer MoS_2 (>200 cm^2/Vs) and WSe_2 (~ 250 cm^2/Vs) with high κ-dielectrics which are studied more recently[19,49]. According to the previous reports[50–53], the mobility could be improved significantly by deposition of high-κ dielectric, such as HfO_2 ($\varepsilon_r = 19$), on the top of 2D materials (graphene or TMDCs) owing to dielectric screening of coulomb scattering on charged impurities. The contact resistance or Schottky barrier could also influence the mobility extraction, and the low contact resistance would enhance the driven current and the electrons mobility by selecting the metal electrode with appropriate work function[15]. However, in our device, Schottky barrier existed in the Au-WS_2 contacts from the non-linear characteristics of output curve. Thus, there is incredible room for improving the mobility of WS_2 nanoflakes FETs by using high-k dielectric and optimizing the contact fabrication. Besides, the multilayer WS_2 nanoflakes FTEs display very small on/off ratio of only 13 times, ascribed to the high off-state current which is attributed to the large thickness of our WS_2 nanoflakes. It is predicted that mono-or few-layer WS_2 would exhibit high field-effect on/off ratio through reducing the off-state current. Therefore, we also fabricated few-layer WS_2 based FETs (Figure S8a). Through the transfer and output characteristics (Figure S8b–c), the few-layer WS_2 FETs exhibit ambipolar properties, the electron and hole mobility are calculated to be 0.47 and 0.79 cm^2/Vs, respectively, and the on/off ratio is significantly improved to be $>10^4$ attributed to the very low off-state current (10^{-11} A) which agrees well with our conjecture. Such results are different and showed higher on/off ratio but lower mobility of few-layer WS_2 compared to the multilayer WS_2 nanoflakes. Further study about the optoelectronic properties of few-layer WS_2 TETs is necessary for the next step.

As discussed above, the incident light field like the electrical field can also modulate the density of carries in the source drain channel and make the multilayer WS_2 nanoflakes be used as ultrasensitive photodetectors with switching on/off ratio of 25 and fast response time of 20 ms. R_λ and EQE are critical parameters for evaluating the quality of photodetctors and large value of R_λ and EQE corresponds to high light-sensibility. R_λ and EQE can be expressed as $R_\lambda = I_{ph}/PS$ and $EQE = hcR_\lambda/e\lambda$, where I_{ph} is the photo-excited current; P is the light power intensity; S is the effective illumination area; h is Planck's constant; c is the velocity of light; e is electron charge; and λ is the excitation wavelength. From our experimental results, under light irradiation (633 nm) of 30 mW/cm^2 with V_{DS} of 1 V, the R_λ and EQE are calculated to be 5.7 A/W and 1118%, respectively, which are three orders of magnitude larger than the photodetectors reported for graphene or single-layer MoS_2[7,33], and even comparable to the reported GaSe and GaS-based photodetctors[13,14]. The high R_λ and EQE are due to a high surface ratio which causes an efficient adsorption of photons. All of the optoelectronic parameters have been compared with those of other 2D materials (Table S1), demonstrating that the multilayer WS_2 nanoflakes have great potential in optoelectronics and highly sensitive photodetectors.

Some theoretical calculations and experimental results about the gas sensing of graphene and MoS_2-based transistors have been reported to demonstrate high sensitive to various gases, and it is pointed out that O_2 and H_2O can act as electron acceptors, whereas NH_3 and ethanol are donors[27,54–57]. In our case, the WS_2 nanoflakes transistors can also response to these given gas molecules. The source drain current of the device is decreased in O_2 and air and increased in ethanol and NH_3, attributed to the charge transfer between the WS_2 nanoflakes and the adsorbed gas molecules, which makes WS_2 nanoflakes can be used in gas sensors. In brief, the multilayer WS_2 nanoflakes are very sensitive to reducing gases, especially NH_3 molecules, but relatively poor sensitive to O_2 molecules. Under light illumina-

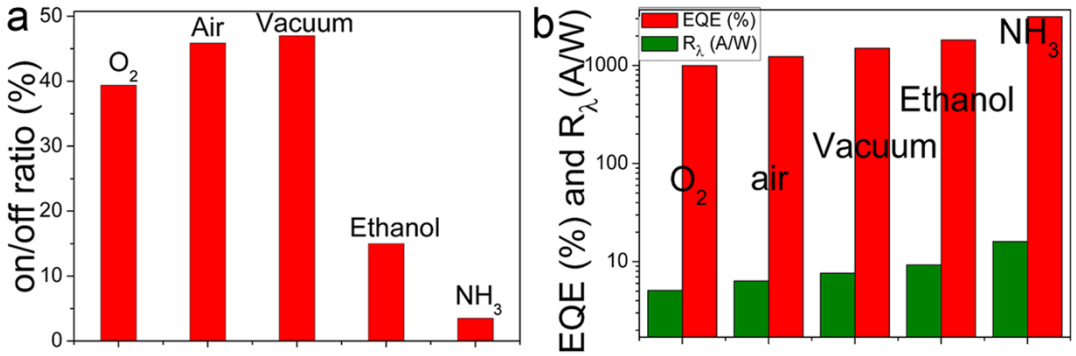

Figure 5 | The effect of gas molecules on photoresponsive parameters. The column diagram of (a) photosensitive on/off ratio, (b) R_λ and EQE of our device based on the multilayer WS_2 nanoflakes at various gas atmospheres. The used incident light is 40 mW/cm^2 with wavelength of 633 nm.

tion, all the gas molecules can be further adsorbed due to the increased electron-hole pairs, and the gas sensitivity is increased for O_2, but decreased for ethanol and NH_3. To our best of knowledge, this is a first report that may create much interest in further study about the gas sensing performance or the mutual influence with light for monolayer WS_2 or other 2D materials.

The gas molecules play an important role in the photosensitive properties. As on/off ratio, R_λ and EQE are critical parameters to evaluate the performance of a phototransistor, the effects of various gas molecules adsorption on the photosensitive properties are demonstrated with these parameters (Figure 5). Table 2 summarizes the performance parameters of our device at different gas atmospheres. The on/off ratio at all the gas atmospheres is lower than that in vacuum (Figure 5a). As mentioned above, poorly O_2 molecules are adsorbed in dark, but the adsorption capacity of O_2 is increased under light illumination. Thus, the reduction of photocurrent outweighs the reduction of dark current, leading to the reduced on/off ratio. As high sensitive gases for our device, the ethanol and NH_3 have been strongly adsorbed in dark, leading to that the dark current becomes very large. When the light illuminates the device, the proportion of increased photocurrent is smaller among the total current, so that the on/off ratio is also decreased. However, the R_λ and EQE of our device are increased significantly in the presence of the ethanol and NH_3 as shown in Figure 5b. The reason is that more ethanol or NH_3 molecules will be adsorbed and donate more electrons when the light illuminated the device, and the number of photo-induced electrons detected per incident photons is overall increased. On the contrary, the oxidizing gases like O_2 serving as electron acceptors will deplete the photo-induced electrons, leading to the decreased R_λ and EQE. Remarkably, the device even reaches a high R_λ of 884 A/W and EQE of 1.7×10^5 % at low illumination power density (50 μW/cm^2) under NH_3 atmosphere.

Our experimental results also indicate that the gas molecules can influence the dependence of photoresponse on illumination intensity and the dynamic response to the light illumination. For example, at NH_3 atmosphere, the dependent exponent α is significantly enhanced into 2.5, implying a high efficiency of photo-generated charge carriers attributed to that more NH_3 molecules can be adsorbed with increased incident light density and more electrons can be transferred from these adsorbates. When the light is switched on, the response to light exhibits two stages including rapid rise and then slow increase process into saturation photocurrent, and the rise photocurrent curve is perfectly fitted by double exponential formula. All the results reveal that two kinds of physical process including the generation of photo-excited electron-hole pairs and charge transfer between the adsorbed gas molecules and the WS_2 nanoflakes play an important role in the efficiency of photo-generated carriers and dynamic response of the device. The reducing gases especially NH_3 would enhance the photosensitivity and efficiency of photo-generated charge carriers, and prolong the response due to their adsorption or desorption with light switching on or off.

To summarize, we report a comprehensive and systematic study about the optoelectronic properties including the field-effect, photosensitive and gas sensing behavior of the multilayer WS_2 nanoflakes. The multilayer WS_2 nanoflakes perform an n-type behavior with electron mobility of 12 cm^2/Vs. The light can serve as "light gating" to modulate the carrier distribution in the WS_2 nanoflakes, and the electrons density and mobility are improved under light illumination. Further, the photosensitive characteristics to red light (633 nm) are performed, and the τ, R_λ and EQE of the multilayer WS_2 nanoflakes photodetectors are <20 ms, 5.7 A/W and 1118%, respectively, demonstrating that the 2D multilayer WS_2 nanoflakes can be effectively used in highly sensitive photodetectors and fast photoelectric switches. Moreover, our devices can response to both oxidizing gas (O_2) and reducing gas (ethanol, NH_3) at room temperature ascribed to the charge transfer between the surface of the WS_2 nanoflakes and physical-adsorbed gas molecules. Under the light illumination, more gas molecules would be adsorbed, and the O_2 molecules acting as "p-dopants" can reduce the R_λ and EQE due to the consumption of photo-excited electrons, while the ethanol and NH_3 molecules acting as "n-dopants" can significantly enhance the R_λ and EQE owing to the contribution of electrons. It is noted that the maximum R_λ and EQE can reach 884 A/W and 1.7×10^5 % respectively under the NH_3 atmospheres, which is highest value of reports so far to our best knowledge. On the other hand, the dynamic response to light under ethanol and NH_3 indicates the existence of two physical mechanisms involving the photo-generation or recombination of electron-hole pairs and gas adsorption or charge transfer. This work would also attract new interests in nanoelectronic and optoelectronic device based on mono- or few-layer WS_2.

Methods

The transistors based on multilayer WS_2 nanoflakes were fabricated with coplanar electrode geometry by "gold-wire mask moving" technique (Figure S9). Firstly, multilayer WS_2 nanoflakes were exfoliated from the WS_2 crystals onto 300 nm SiO_2/Si substrates using mechanical exfoliation technique, and with vacuum-annealing at 350°C for 2 hours to remove the residual glue. Secondly, a micron

Table 2 | Performance parameters (on/off ratio, R_λ and EQE) of the phototransistors based on the multilayer WS_2 nanoflakes under light illumination (633 nm, 40 mW/cm^2) at various gas atmospheres

Parameters	O_2	Air	Vacuum	Ethanol	NH_3
On/off ratio	39	46	47	15	3.5
R_λ (A/W)	5.1	6.4	7.7	9.3	16.1
EQE (%)	999	1235	1500	1823	3146

gold-wire serving as a mask was fixed tightly on the top surface of WS_2 nanoflakes, and then a pair of Au electrodes was deposited onto the substrate by thermal evaporation. To avoid the scattering of metallic atoms onto the side-face of SiO_2/Si substrates, the sides of the substrate were covered with tinfoil. Moreover, the distance between the thermal evaporation boat and the sample was increased to 15 cm and the deposition rate was controlled at around 0.5 Å/s in order to minimize the heat influence. Finally, by slightly removing the Au wire mask and tinfoil, the Au electrodes were fabricated and a micron size gap was produced between the two electrodes.

1. Geim, A. K. Graphene: Status and Prospects. *Science* **324**, 1530–1534 (2009).
2. Avouris, P., Chen, Z. & Perebeinos, V. Carbon-based electronics. *Nat. Nanotechnol.* **2**, 605–615 (2007).
3. Rao, N. R., Sood, A. K., Subrahmanyam, K. S. & Govindaraj, A. Graphene: the new two-dimensional nanomaterial. *Angew. Chem. Int. Ed.* **48**, 7752–7777 (2009).
4. Schwierz, F. Graphene transistors. *Nat. Nanotechnol.* **5**, 487–496 (2010).
5. Elias, D. C. *et al.* Dirac cones reshaped by interaction effects in suspended graphene. *Nature Phys.* **7**, 701–704 (2011).
6. Geim, A. K. & Novoselov, K. S. The rise of graphene. *Nature Mater.* **6**, 183–191 (2007).
7. Xia, F., Mueller, T., Lin, Y., Valdes-Garcia, A. & Avouris, P. Ultrafast graphene photodetector. *Nat. Nanotechnol.* **4**, 839–843 (2009).
8. Khan, M. A., Kuznia, J. N., Olson, D. T., Blasingame, M. & Bhattarai, A. R. Schottky-barrier photodetector based on Mg-Doped P-type GaN films. *Appl. Phys. Lett.* **63**, 2455–2456 (1993).
9. Wilson, J. A. & Yoffe, A. D. Transition metal dichalcogenides: discussion and interpretation of observed optical, electrical and structural properties. *Adv. Phys.* **18**, 193–335 (1969).
10. Yoffe, A. D. Layer compounds. *Annu. Rev. Mater. Sci.* **3**, 147–170 (1993).
11. Tsai, D. S. *et al.* Few-Layer MoS_2 with High Broadband Photogain and Fast Optical Switching for Use in Harsh Environments. *ACS Nano* **7**, 3905–3911 (2013).
12. Tongay, S. *et al.* Broad-Range Modulation of Light Emission in Two-Dimensional Semiconductors by Molecular Physisorption Gating. *Nano Lett.* **13**, 2831–2836 (2013).
13. Hu, P. A. *et al.* Highly Responsive Ultrathin GaS Nanosheet Photodetectors on Rigid and Flexible Substrates. *Nano Lett.* **13**, 1649–1654 (2013).
14. Hu, P. A., Wen, Z., Wang, L., Tan, P. & Xiao, K. Synthesis of Few-Layer GaSe Nanosheets for High Performance Photodetectors. *ACS Nano* **6**, 5988–5994 (2012).
15. Liu, W. *et al.* Role of Metal Contacts in Designing High-Performance Monolayer n-Type WSe_2 Field Effect Transistors. *Nano Lett.* **13**, 1983–1990 (2013).
16. Mak, K., He, K., Shan, J. & Heinz, T. F. Control of valley polarization in monolayer MoS_2 by optical helicity. *Nat. Nanotechnol.* **7**, 494–498 (2012).
17. Podzorov, V., Gershenson, M. E., Kloc, C., Zeis, R. & Bucher, E. High-mobility field-effect transistors based on transition metal dichalcogenides. *Appl. Phys. Lett.* **84**, 3301–3303 (2004).
18. Ayari, A., Cobas, E., Ogundadegbe, O. & Fuhrer, M. S. Realization and electrical characterization of ultrathin crystals of layered transition-metal dichalcogenides. *J. Appl. Phys.* **101**, 014507 (2007).
19. Radisavljevic, B., Radenovic, A., Brivio, J., Giacometti, V. & Kis, A. Single-layer MoS_2 transistors. *Nat. Nanotechnol.* **6**, 147–150 (2011).
20. Mueller, T., Xia, F. & Avouris, P. Graphene photodetectors for high-speed optical communications. *Nat. Photonics* **4**, 297–301 (2010).
21. Nair, R. R. *et al.* Fine Structure Constant Defines Visual Transparency of Graphene. *Science* **320**, 1308–1308 (2008).
22. Lopez-Sanchez, O., Lembke, D., Kayci, M. & Kis, A. Ultrasensitive photodetectors based on monolayer MoS_2. *Nat. Nanotechnol.* **8**, 497–501 (2013).
23. Xue, D. J. *et al.* Anisotropic Photoresponse Properties of Single Micrometer-Sized GeSe Nanosheet. *Adv. Mater.* **24**, 4528–4533 (2012).
24. Late, D. J. *et al.* GaS and GaSe Ultrathin Layer Transistors. *Adv. Mater.* **24**, 3549–3554 (2012).
25. Li, H. *et al.* Fabrication of single- and multilayer MoS_2 film-based field-effect transistors for sensing NO at room temperature. *Small* **8**, 63–67 (2012).
26. He, Q. *et al.* Fabrication of flexible MoS_2 thin-film transistor arrays for practical gas-sensing applications. *Small* **8**, 2994–2999 (2012).
27. Late, D. J. *et al.* Sensing Behavior of Atomically Thin-Layered MoS_2 Transistors. *ACS Nano* **7**, 4879–4891 (2013).
28. Perkins, F. K. *et al.* Chemical Vapor Sensing with Monolayer MoS_2. *Nano Lett.* **13**, 668–673 (2013).
29. Brainard, W. A. *The Thermal Stability And Friction Of The Disulfides, Diselenides, And Ditellurides Of Molybdenum And Tungsten In Vacuum (10^{-9} to 10^{-6} torr).* NASA, Washington, 1969.
30. Prasad, S. V., McDevitt, N. T. & Zabinski, J. S. Tribology of tungsten disulfide-nanocrystalline zinc oxide adaptive lubricant films from ambient to 500°C. *Wear* **237**, 186–196 (2000).
31. Leitao, L., Kumar, S. B., Yijian, O. & Jing, G. Performance Limits of Monolayer Transition Metal Dichalcogenide Transistors. *IEEE Trans. Electron Devices* **58**, 3042–3047 (2011).
32. Hwang, W. S. *et al.* Transistors with chemically synthesized layered semiconductor WS_2 exhibiting 10^5 room temperature modulation and ambipolar behavior. *Appl. Phys. Lett.* **101**, 013107 (2012).
33. Yin, Z. *et al.* Single-layer MoS_2 phototransistors. *ACS Nano* **6**, 74–80 (2012).
34. Kuc, A., Zibouche, N. & Heine, T. Influence of quantum confinement onthe electronic structure of the transition metal sulfide TS_2. *Phys. Rev. B* **83**, 245213 (2011).
35. Tang, Q. *et al.* Low Threshold Voltage Transistors Based on Individual Single-Crystalline Submicrometer-Sized Ribbons of Copper Phthalocyanine. *Adv. Mater.* **18**, 65–68 (2006).
36. Tang, Q., Li, H., Liu, Y. & Hu, W. High-Performance Air-Stable n-Type Transistors with an Asymmetrical Device Configuration Based on Organic Single-Crystalline Submicrometer/Nanometer Ribbons. *J. Am. Chem. Soc.* **128**, 14634–14639 (2006).
37. Elías, A. L. *et al.* Controlled Synthesis and Transfer of Large-Area WS_2 Sheets: From Single Layer to Few Layers. *ACS Nano* **7**, 5235–5242 (2013).
38. Frey, G. L., Tenne, R., Matthews, M. J., Dresselhaus, M. S. & Dresselhaus, G. Optical Properties of MS_2 (M = Mo, W) Inorganic Fullerene-like and Nanotube Material Optical Absorption and Resonance Raman Measurements. *J. Mater. Res.* **13**, 2412–2417 (1998).
39. Berkdemir, A. *et al.* Identification of Individual and Few Layers of WS_2 Using Raman Spectroscopy. *Sci. Rep.* **3**, 1755 (2013).
40. Fivaz, R. & Mooser, E. Mobility of charge carriers in semiconducting layer structures. *Phys. Rev.* **163**, 743–755 (1967).
41. Sze, S. M. & Kwok, K. Ng. *Physics Of Semiconductors Devices.* John Wiley & Sons, Hoboken, 2006.
42. Carlos, G. M. & Márcio, C. S. *MOSFET Modeling For Circuit Analysis And Design.* World Scientific. Singapore, 2007.
43. Zhang, W. *et al.* High-Gain Phototransistors Based on a CVD MoS_2 Monolayer. *Adv. Mater.* **25**, 3456–3461 (2013).
44. Konstantatos, G. *et al.* Hybrid graphene-quantum dot phototransistors with ultrahigh gain. *Nat. Nanotechnol.* **7**, 363–368 (2012).
45. Jeon, S. *et al.* Gated three-terminal device architecture to eliminate persistent photoconductivity in oxide semiconductor photosensor arrays. *Nature Mater.* **11**, 301–305 (2012).
46. Zhang, C. *et al.* High-performance photodetectors for visible and near-infrared lights based on individual WS_2 nanotubes. *Appl. Phys. Lett.* **100**, 243101 (2012).
47. Lee, Y. H. *et al.* Synthesis and Transfer of Single-Layer Transition Metal Disulfides on Diverse Surfaces. *Nano Lett.* **13**, 1852–1857 (2013).
48. Novoselov, K. S. *et al.* Two-dimensional atomic crystals. *Proc. Natl Acad. Sci. USA* **102**, 10451–10453 (2005).
49. Fang, H. *et al.* High-performance single layered WSe_2 p-FETs with chemically doped contacts. *Nano Lett.* **12**, 3788–3792 (2012).
50. Jena, D. & Konar, A. Enhancement of carrier mobility in semiconductor nanostructures by dielectric engineering. *Phys. Rev. Lett.* **98**, 136805 (2007).
51. Konar, A., Fang, T. & Jena, D. Effect of high-κ gate dielectrics on charge transport in graphene-based field effect transistors. *Phys. Rev. B* **82**, 115452 (2010).
52. Newaz, A. K. M., Puzyrev, Y. S., Wang, B., Pantelides, S. T. & Bolotin, K. I. Probing charge scattering mechanisms in suspended graphene by varying its dielectric environment. *Nature Commun.* **3**, 734 (2012).
53. Chen, F., Xia, J., Ferry, D. K. & Tao, N. Dielectric screening enhanced performance in graphene FET. *Nano Lett.* **9**, 2571–2574 (2009).
54. Leenaerts, O., Partoens, B. & Peeters, F. M. Adsorption of H_2O, NH_3, CO, NO_2, and NO on graphene: A first-principles study. *Phys. Rev. B* **77**, 125416 (2008).
55. Yuan, W. & Shi, G. Graphene-based gas sensors. *J. Mater. Chem. A* **1**, 10078–10091 (2013).
56. Schedin, F. *et al.* Detection of individual gas molecules adsorbed on graphene. *Nature Mater.* **6**, 652–655 (2007).
57. Yue, Q., Shao, Z., Chang, S. & Li, J. Adsorption of gas molecules on monolayer MoS_2 and effect of applied electric field. *Nanoscale Res. Lett.* **8**, 425 (2013).

Acknowledgments

This work was supported by the National Natural Science Foundation of China under Grant No.91233120 and the National Basic Research Program of China (2011CB921901).

Author contributions

N.H. and J.L. conceived the project. N.H. performed the measurements. Z.W. performed AFM measurements. S.Y., Z.W., S.S.L., J.B.X. and J.L. edited the manuscript. N.H. and J.L. wrote the manuscript. All authors have read the manuscript.

Additional information

Supplementary information accompanies this paper at http://www.nature.com/scientificreports

Competing financial interests: The authors declare no competing financial interests.

How to cite this article: Huo, N. *et al.* Photoresponsive and Gas Sensing Field-Effect Transistors based on Multilayer WS_2 Nanoflakes. *Sci. Rep.* **4**, 5209; DOI:10.1038/srep05209 (2014).